

## Retraction

# Retracted: Dance Motion Capture Based on Data Fusion Algorithm and Wearable Sensor Network

### Complexity

Received 19 December 2023; Accepted 19 December 2023; Published 20 December 2023

Copyright © 2023 Complexity. This is an open access article distributed under the Creative Commons Attribution License, which permits unrestricted use, distribution, and reproduction in any medium, provided the original work is properly cited.

This article has been retracted by Hindawi following an investigation undertaken by the publisher [1]. This investigation has uncovered evidence of one or more of the following indicators of systematic manipulation of the publication process:

- (1) Discrepancies in scope
- (2) Discrepancies in the description of the research reported
- (3) Discrepancies between the availability of data and the research described
- (4) Inappropriate citations
- (5) Incoherent, meaningless and/or irrelevant content included in the article
- (6) Manipulated or compromised peer review

The presence of these indicators undermines our confidence in the integrity of the article's content and we cannot, therefore, vouch for its reliability. Please note that this notice is intended solely to alert readers that the content of this article is unreliable. We have not investigated whether authors were aware of or involved in the systematic manipulation of the publication process.

In addition, our investigation has also shown that one or more of the following human-subject reporting requirements has not been met in this article: ethical approval by an Institutional Review Board (IRB) committee or equivalent, patient/participant consent to participate, and/or agreement to publish patient/participant details (where relevant).

Wiley and Hindawi regrets that the usual quality checks did not identify these issues before publication and have since put additional measures in place to safeguard research integrity.

We wish to credit our own Research Integrity and Research Publishing teams and anonymous and named external researchers and research integrity experts for contributing to this investigation.

The corresponding author, as the representative of all authors, has been given the opportunity to register their agreement or disagreement to this retraction. We have kept a record of any response received.

### References

- [1] Y. Li, "Dance Motion Capture Based on Data Fusion Algorithm and Wearable Sensor Network," *Complexity*, vol. 2021, Article ID 2656275, 11 pages, 2021.

## Research Article

# Dance Motion Capture Based on Data Fusion Algorithm and Wearable Sensor Network

Yueru Li 

Graduate School of Shinhan University, Seoul 11655, Republic of Korea

Correspondence should be addressed to Yueru Li; 20132134447@mail.sdufe.edu.cn

Received 29 April 2021; Revised 8 June 2021; Accepted 16 June 2021; Published 23 June 2021

Academic Editor: Zhihan Lv

Copyright © 2021 Yueru Li. This is an open access article distributed under the Creative Commons Attribution License, which permits unrestricted use, distribution, and reproduction in any medium, provided the original work is properly cited.

In this paper, through an in-depth study and analysis of dance motion capture algorithms in wearable sensor networks, the extended Kalman filter algorithm and the quaternion method are selected after analysing a variety of commonly used data fusion algorithms and pose solving algorithms. In this paper, a sensor-body coordinate system calibration algorithm based on hand-eye calibration is proposed, which only requires three calibration poses to complete the calibration of the whole-body sensor-body coordinate system. In this paper, joint parameter estimation algorithm based on human joint constraints and limb length estimation algorithm based on closed joint chains are proposed, respectively. The algorithm is an iterative optimization algorithm that divides each iteration into an expectation step and a great likelihood step, and the best convergence value can be found efficiently according to each iteration step. The feature values of each pose action are fed into the algorithm for model learning, which enables the training of the model. The trained model is then tested by combining the collected gesture data with the algorithmic model to recognize and classify the gesture data, observe its recognition accuracy, and continuously optimize the model to achieve accurate recognition of human gesture actions.

## 1. Introduction

Based on human motion capture and recognition, body-sensitive interactive games have revolutionised the traditional game industry. This kind of somatosensory game completely breaks the bondage of the handle button, using the human motion capture device to capture the gamer's movement and directly use it as the game's input to control the game character's movement [1]. This game method greatly enhances the player's sense of participation, making the game more realistic and interesting, bringing a new game experience to gamers, and promising to become the future direction of game development. Somatosensory games integrate games and fitness into one, allowing gamers to get fit in entertainment and entertain in fitness, killing two birds with one stone. Motion capture is a technology that uses corresponding sensors to sample the motion data of a target object, record its motion process, and then process the data through a computer to finally achieve functions such as restoration display, classification modelling, or analysis

research of the object's motion [2]. In some cases, motion capture treats the target moving object as a whole and records only its movement trajectory in three-dimensional space, so it is also called motion tracking, while in some special application scenarios, it may need to record extremely complex motion information, such as human facial expressions, swelling changes of objects, and it is usually called performance capture when such tiny and precise expressions need to be captured [3].

With the rapid development of computer technology and the rapid change of peripherals for data acquisition, motion capture technology has become increasingly mature, and many consumer-grade products have been successfully used in military, entertainment, medical, sports, and autonomous driving industries, creating huge production and research value [4]. As a frontier technology with great commercial potential and wide application areas, the technical research of motion capture is of great significance. In this paper, the application scenarios of motion capture are broadly classified into two categories, motion analysis and

device interaction, and are briefly introduced separately. Motion analysis allows one to learn the motion patterns of target objects and use them for analytical modelling. For example, in the field of medical rehabilitation, remote monitoring networks can be established for patients to enhance the monitoring of their behaviour and thus provide timely feedback on medical data; in the field of ergonomics, it can also provide sufficiently accurate human posture data for research [5]; in the field of sports, motion analysis technology can be used to simulate training, record athletes' movement data and compare them with standard templates to generate corrective information for reference; in the entertainment film and television industry, motion analysis technology can be used to record athletes' movement data and compare them with standard templates to generate corrective information for reference. In the entertainment film and television industry, motion analysis techniques are used in 3D graphics production to restore the movements of the target object, and lifelike character modelling can be obtained [6]. Along with the development of these posture recognition technologies and the national promotion of the Internet of Things, there is a growing need for such wearable posture recognition devices for many jobs in life. On the one hand, outdoor activities are dangerous, and wearable posture recognition devices can predict some dangerous movements to avoid accidents as much as possible and ensure the safety of workers; on the other hand, through the staff's long-time posture data collection, analysing their various working postures can effectively improve the work efficiency.

In response to the abovementioned needs in terms of posture recognition, new posture recognition technologies are continuously researched and developed, which improve the vacancy of such technologies, improve people's work efficiency, and greatly reduce the danger in some work, which is of great significance to the development of society. Human motion capture technology can directly obtain the kinematic data and parameters of the human body, and these parameters can be used to assist in the development and design of prostheses and provide the basis for the debugging of motion control parameters of assisted robots and bipedal humanoid robots. The use of human motion can realize remote control of robots, which is flexible in operation compared with traditional remote-control methods, especially for humanoid robotic arms, and can realize fine and complex manipulation operations. In the field of identification and security, human gait recognition based on human motion capture has become a new biometric identification technology. In personal navigation and positioning, personal positioning and navigation are achieved by continuous measurement of human lower limb movement trajectories. This positioning method does not rely on external signals and is highly covert and can be used in confined environments such as indoors, tunnels, and underground cities.

## 2. Status of Research

Abhinav Gupta et al. proposed a Bayesian network recognition algorithm combining video data and image data, which combines various factors such as scene, object, action,

and object response to enhance the global connectivity of different elements, thus improving the recognition performance of the basic elements [7]. St-Onge proposed an algorithm using the 3D angle of human joints algorithm for pose recognition [8]. By mapping the pose information obtained from the stereo camera to a series of discrete symbols required by the implicit Markov model, the trained results show that this method has a better recognition rate than the traditional methods, especially for the poses that cannot be recognized under the traditional methods [9]. Switonski et al. developed a mobile platform that can be used for human pose recognition, solving the problem of device processing power and energy consumption that exists in mobile devices, with the MECLA Cook efficient evaluation of classification algorithms, while the platform is designed with applications dedicated to body domain networks [10]. Malik et al. combined a human kinematic model based on the Kalman filter to separate gravitational and linear accelerations from accelerometer measurements and use gravitational acceleration estimation to calculate the tilt angle of the limb, which is superior to the low-pass filter-based processing [11]. Due to the linear acceleration, accelerometer-based human motion capture systems are only suitable for stationary or slow-moving situations, and the measurement error increases significantly when the human body is moving vigorously [12]. Also, even without the interference of linear acceleration, the accelerometer can only measure two rotational degrees of freedom and cannot be used for the measurement of the multirotational degree of freedom joints [13].

For inertial motion capture systems, the motion capture accuracy is determined by a combination of factors. First, high accuracy and low latency limb pose measurement is the basis of human motion capture and reconstruction. The pose measurement based on MEMS inertial sensors is not only affected by sensor measurement errors and noise, but also by the linear acceleration of human motion and magnetic interference from the surrounding environment [14]. Therefore, a combination of multisensor fusion algorithms is required to obtain accurate and stable pose measurements. Second, due to the irregularity of the human limb surface, it is difficult to ensure that the measurement coordinate system of the sensor coincides exactly with the limb coordinate system of the human body when the sensor is worn, so the sensor measurement needs to be converted to the human body coordinate system by initialization calibration. If there is an error in the initial calibration of the coordinate system, or if the sensor is shifted relative to the human body during the motion, in this case, even if there is no error in the pose measurement of the MEMS inertial sensor, the human motion capture will be distorted. Finally, in human motion reconstruction, the limb parameters of the captured object need to be determined [15]. If the skeletal length of the captured object is different from that of the virtual 3D human, the motion reconstruction will be distorted, for example, if the foot hangs or wears the ground, or if the limb crosses the torso.

The human body is simplified into a hierarchical chain skeletal model consisting of 15 bones and 14 joints based on

its structural and kinematic characteristics. To mathematically describe the motion state of each limb, a coordinate system is established and the rotation matrix, Euler angles, and quaternions are introduced for the description of the spatial pose of the limb. By analysing the motion of the main joints of the human body, the rotational degrees of freedom constraints of each joint and the joint rotation angle range limits are added to the human skeletal model. Multisensor fusion-based pose and position measurement, system initialization calibration, and human motion recognition: multisensor fusion-based attitude and position measurement is the basis of the study. The multisensor fusion algorithm is used to fuse data from multiple sensors to obtain accurate and reliable attitude and position measurements. The initial calibration of the system consists of two main aspects: the first aspect is the calibration of the rotation matrix between the sensor measurement coordinate system and the human coordinate system, also called sensor-human coordinate system calibration; the other aspect is the human body parameter estimation, which is used for the correction of the 3D virtual human model parameters. Human motion recognition is the recognition of human motion patterns based on human motion capture data.

### 3. Analysis of Dance Motion Capture by the Wearable Sensor Network

**3.1. Wearable Sensor Network Design.** With the increasing maturity of micromechanical electronic system technology, MEMS inertial sensors have obvious progress in size, weight, and price, but in a short period, MEMS inertial sensors are still difficult to obtain a significant improvement in measurement accuracy and stability. According to the cause and nature of the measurement error of MEMS inertial sensor, it can be divided into deterministic error and random error. Deterministic errors are caused by the manufacturing material and processing process of the sensor, for example, measurement axis nonorthogonal error, scale factor error, and zero-bias error [16]. Said data processing platform includes an intelligent mobile terminal device, a personal computer, and a cloud server, said intelligent mobile terminal device and personal computer being connected to said wearable sensor by wireless communication via said wireless communication module, respectively, and said cloud server being connected to said intelligent mobile terminal device and personal computer by network communication, respectively. Uncertainty errors are random drifts caused by uncertainties, such as ambient temperature and humidity, and these errors are difficult to separate from the measurement signal.

Ideally, the three measurement axes of the sensor are orthogonal to each other. In fact, due to various factors in the processing and manufacturing of the sensor as well as in the installation process, the three measurement axes deviate from the orthogonal coordinate axes, and the mathematical model of the nonorthogonal error of the measurement axes is

$$\begin{bmatrix} X_1 \\ Y_1 \\ Z_1 \end{bmatrix} = \begin{bmatrix} \sin \alpha \cos \gamma & \sin \beta & \cos \gamma \sin \gamma \\ 0 & \cos \alpha \sin \beta & \cos \beta \sin \alpha \\ 0 & 0 & 0 \end{bmatrix} \begin{bmatrix} X_0 \\ Y_0 \\ Z_0 \end{bmatrix}, \quad (1)$$

where  $\alpha$ ,  $\beta$ , and  $\gamma$  are the deviation angles of the  $X$ -axis,  $Y$ -axis, and  $Z$ -axis, respectively. Most of the MEMS inertial sensors on the market today are three-axis integrated or even nine-axis integrated sensors, and the nonorthogonal error of the measurement axes caused by the manufacturing process and installation is almost negligible [17]. The scale factor error is the measurement error caused by the inconsistent sensitivity of each measurement axis, mainly caused by the fact that signal conditioning circuit (amplifier) characteristics of each measurement axis are not the same. The scale factor error matrix is a  $3 \times 3$  diagonal matrix, which ideally should be a unit matrix. The mathematical model of the scale factor error is

$$\begin{bmatrix} X_2 \\ Y_2 \\ Z_2 \end{bmatrix} = \begin{bmatrix} s_x & 1 & 0 \\ 0 & s_y & 1 \\ 1 & 0 & s_z \end{bmatrix} \begin{bmatrix} X_1 \\ Y_1 \\ Z_1 \end{bmatrix}, \quad (2)$$

where  $s_x$ ,  $s_y$ , and  $s_z$  are the scale factors corresponding to the three measurement axes, respectively. The zero-bias error is the error caused by the nonzero zero points of the sensor's analogy circuit or A/D conversion circuit, and its mathematical model is

$$\begin{bmatrix} X \\ Y \\ Z \end{bmatrix} = \begin{bmatrix} X_2 \\ Y_2 \\ Z_2 \end{bmatrix} - \begin{bmatrix} b_x \\ b_y \\ b_z \end{bmatrix} = \begin{bmatrix} X_2 - b_x \\ Y_2 - b_y \\ Z_2 - b_z \end{bmatrix}, \quad (3)$$

where  $b_x$ ,  $b_y$ , and  $b_z$  are the zero-bias errors of the  $X$ -axis,  $Y$ -axis, and  $Z$ -axis, respectively. The measurement of the gyroscope is not easily affected by the external environment (magnetic field) and the motion state of the carrier (stationary, uniform motion, nonuniform motion, etc.), with good dynamic performance and high instantaneous accuracy, which can quickly track and measure the change of carrier attitude. Under the condition that the initial attitude of the carrier is known, the integration of the angular rate output from the gyroscope can get the attitude of the carrier. Due to the zero-bias error and random drift of the gyroscope measurement, the accumulated error will become larger and larger over time, which eventually leads to the dispersion of the attitude measurement. Therefore, using a gyroscope alone for attitude estimation can only obtain a more reliable attitude estimation in a very short period and cannot obtain a long time and high accuracy attitude measurement. The main contribution of this manuscript is the new algorithm.

The transport layer refers to the convergence layer that gets all kinds of body domain network information for preliminary processing and then transmits the data to the server for processing carrier. The server is set up at the remote end as the user's data centre to classify, process, and store the data. The transmission layer is mainly reflected in the transmission mode of data, which can be built by existing

transmission modes such as base station and Wi-Fi to build a bridge between the aggregation layer and the storage layer.

The storage layer is a brand-new challenge for the development of the body area network so far. With the increasing number of users and network complexity, the amount of data becomes huge. How to efficiently, quickly, and accurately complete the process of storing and processing a huge amount of data is the key to realize the application of today's body domain network system. At the same time, the process can establish a proprietary electronic data file for users and according to the demand can realize the cloud upload and download function, and thanks to the current rapid development of cloud computing and cloud storage technology, users can realize long-term status monitoring following the body area network monitoring data, which undoubtedly extends the richness of wireless body area network, as shown in Figure 1.

WABAN user-side wireless sensor nodes are roughly divided into three types according to their distribution in the human body, as shown in Figure 1, which are sensor nodes implanted in the human body, sensor nodes distributed on the surface of the human body, and sensor nodes located around the human body closer to the human body [18]. Each type of node accomplishes its monitoring function according to different characteristics, and the sensor nodes implanted in the body mainly include insulin pumps and pacemakers; the sensor nodes distributed on the surface of the human body mainly include body temperature, pulse, and heart rate sensors; the sensors located closer to the human body mainly include inhalation pill temperature measurement sensors and EEG scanners.

Although the principle of the six-sided calibration method is simple, it is difficult to operate in practice. Firstly, we need to use the instrumentation to determine the direction of local gravitational acceleration; secondly, it is difficult to ensure that the positive and negative measurement axes coincide exactly with the direction of gravitational acceleration during the placement of the accelerometer. In the calibration process, a single problem will cause the calibration to fail. This calibration method requires high accuracy of the measurement equipment and is complicated to operate, which is counterproductive if the operation is not standard. To improve the accuracy of calibration experiments, this paper adopts an ellipsoid-based accelerometer calibration algorithm, which is simple to operate and does not require additional equipment. In the stationary state, the linear acceleration of the carrier is zero, and the measurement model of the accelerometer in (4) can be simplified as

$$G_p = \frac{S_a g_b - b_a + v_a}{S_a g_b + b_a - v_a}, \quad (4)$$

where  $G_p$  is the projection of the gravitational acceleration in the sensor measurement coordinate system, i.e.,  $g_b = R_{eb}^T g_e$ .

Magnetometer measurements are disturbed not only by their instrumentation errors, but also by the interference of the magnetic field generated by the magnetic material around the carrier. According to the nature of the magnetic field, interference sources can be divided into two categories:

hard magnetic interference errors and soft magnetic interference errors. To improve the accuracy and reliability of attitude measurement, the instrumentation error of the magnetometer and the hard and soft magnetic interference errors need to be calibrated and compensated before data fusion. Hard magnetic interference error is the error caused by the magnetometer being disturbed by the magnetic field generated by the magnetic substance on the carrier. This magnetic substance has a relatively high remanence and can produce a fixed magnetic field that is not affected by external magnetic fields and does not change with time and position, such as permanent magnets. Since the strength and direction of the interfering magnetic field remain constant, hard magnetic interference causes a fixed bias in the measurement output of the magnetometer, whose value does not change with time and can be considered as a zero-bias error. The soft magnetic material can be excited by an external magnetic field to produce a magnetic field that varies with the size and direction of the external field. This measurement error caused by the magnetic field generated by the soft iron material magnetized by the external magnetic field is called soft magnetic interference error. In general, we assume that the soft magnetic interference error is linear with the external magnetic field and has no hysteresis, so the soft magnetic error matrix is a  $3 \times 3$  symmetric matrices, i.e.,

$$C_{si} = \begin{bmatrix} \alpha_{11} & 0 & 1 \\ 1 & \alpha_{22} & 0 \\ 0 & 1 & \alpha_{33} \end{bmatrix}. \quad (5)$$

Considering the scale factor error, zero-bias error, and hard and soft magnetic interference error, the measurement error model of the magnetometer is

$$B_p = \frac{S_m C_{si} (B_b + b_{hi}) - b_m + v_m}{b_m - v_m}, \quad (6)$$

where  $b_{hi}$  is the hard magnetic interference error.

Most of the data transmission modules on the market today are 4G modules because of the fast data transmission speed and the simplicity and convenience of using AT commands in the software design, but the drawback is the large power consumption. The MT2503 supports GPRS/GSM communication, and the main control board is designed with a SIM card module that can send data to the server to save the processed attitude data. As shown in Figure 2, a 6-pin Micro-SIM package is used in the schematic design to save the PCB footprint.

We can add more sensors, because the more the sensors, the smaller the blind spot. But to deal with the large amount of fuzzy data generated, the corresponding mathematical processing becomes more difficult. The emergence of modern sensor fusion algorithms has just solved the problem of multiple sensor data processing. The purpose of the whole set of equipment is to collect human posture information, to avoid affecting the normal posture of the human body; the size of the circuit board should be designed as small as possible circuit board design into a six-layer board, size  $5 * 4$  cm, respectively: the top layer, bottom

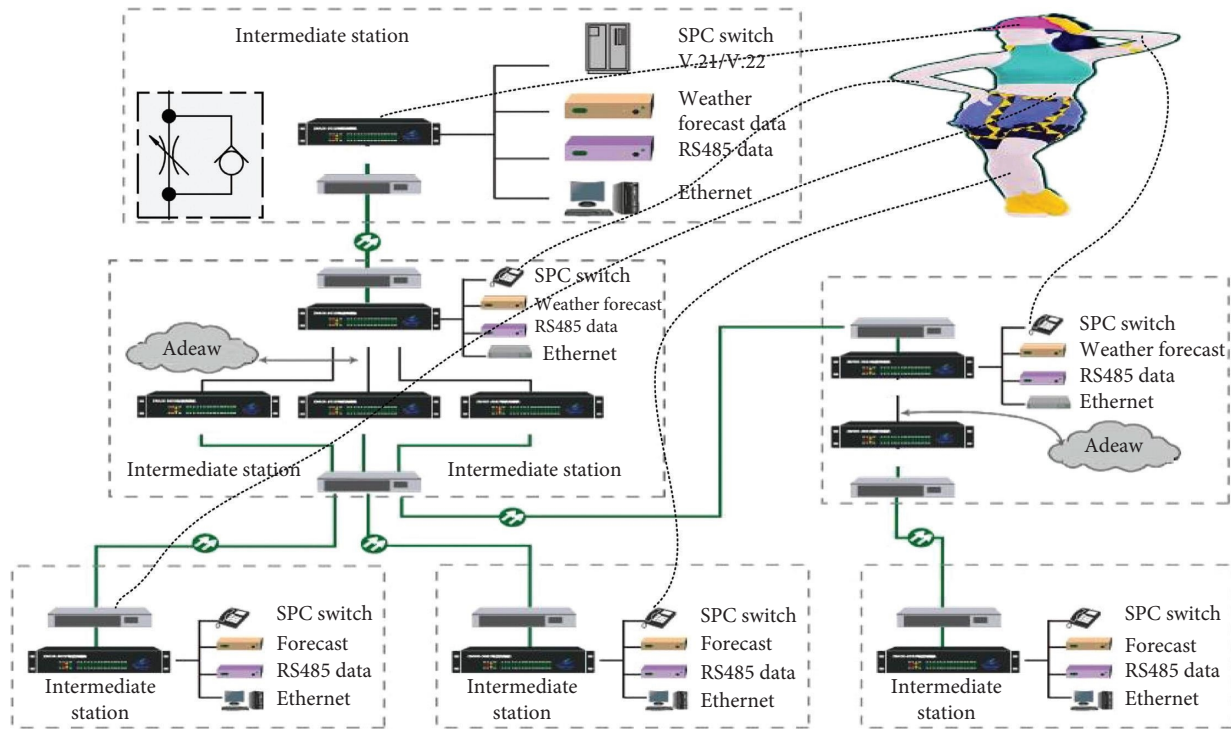


FIGURE 1: WABAN network architecture diagram.

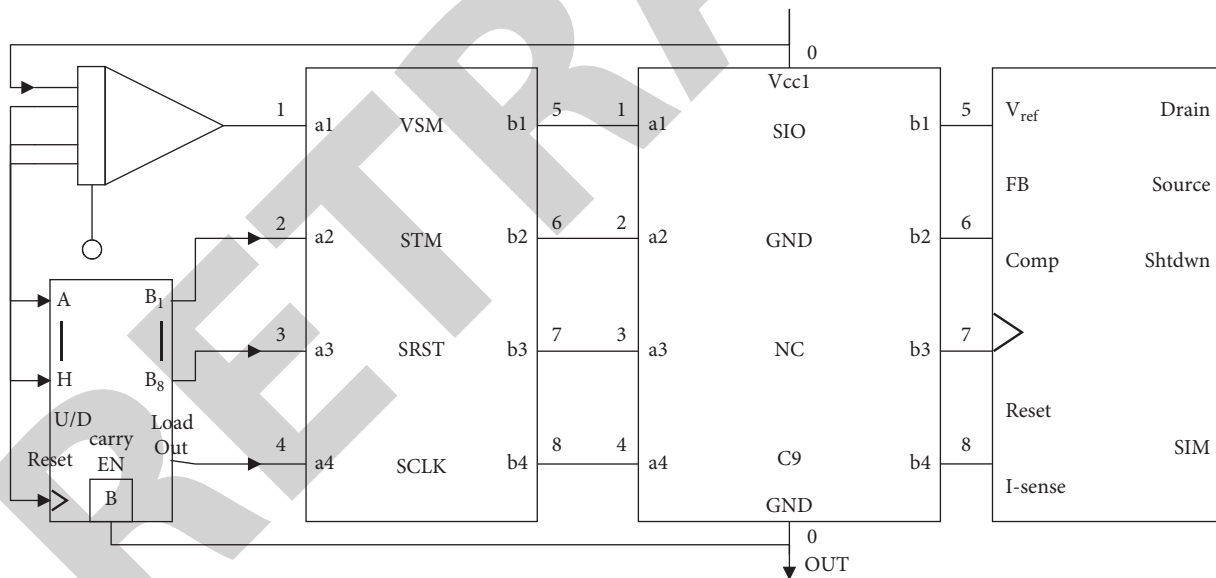


FIGURE 2: SIM card module.

layer, power layer, ground layer, and two signal layers. Components are placed in the top and bottom layers; three antenna holders are designed in the edge part of the board, while the periphery is as far as possible without digital signal lines; MT2503 chip and peripheral crystal circuit design are in the top layer of the board; SIM card holders are designed in the bottom layer of the board, away from the metal part, to avoid interference in the process of sending data, resulting in the loss of data in the upload.

The accelerometer and gyroscope in the ICM-20948 chip can be activated by triggering the self-test register, and the chip will automatically simulate the external force applied to the accelerometer and gyroscope after the self-test. After the self-test, the output value will change compared to the value without the self-test state. When the self-test function is activated, the sensor will generate an output signal to observe the self-test condition, and the self-test response value is equal to the difference between the

sensor output value with self-test and the output value without self-test. When the self-test response value is within a reasonable range, the self-test will pass; when the self-test response value is outside the specified range, it indicates that the self-test has failed.

**3.2. Analysis of Dance Motion Capture Algorithm.** Different features are also usually extracted for data with different action types. Usually, signal features can be divided into time-domain features and frequency domain features. Time-domain features are features extracted directly from the sequence of acceleration data. This extraction method is simple and effective, with a small computational effort, and commonly used methods include peak-to-peak values, combined acceleration, and waveform information. Frequency domain features are firstly the Fourier transform of the time-domain signal, and then the features are extracted in the frequency domain [19–21]. The commonly used frequency domain features are FFT transform, wavelet transform, and discrete cosine transform. In the complex motion data of the human body, it is necessary to analyse the features of each action to train and recognize each action.

At the stage of double foot support, when ready to start walking, the body tends to walk forward, the acceleration in the vertical up and down direction and the front and back direction is positive, and the acceleration is increasing; when the body is tilted forward to the maximum, the acceleration also reaches the peak; then the right heel is raised, the right knee is bent, the body is in the right foot movement stage, and the acceleration fluctuates in the vertical direction. Now when the right foot is lifted off the ground, it is in the left foot support phase, and when the body is standing vertically, the acceleration in the vertical direction reaches its maximum, and according to the way the human body walks, it will tend to go left or right in the air, and there will be an acceleration generated in the left and right directions [22–25]. When the right foot hits the ground, it will be in the stage of double foot support again, the left foot starts to lift, and the acceleration fluctuates in the vertical direction; when in the stage of standing on the right leg, the acceleration in the vertical direction is changing and gradually restoring the vertical standing, and the acceleration also reaches the maximum. The acceleration of the walking motion will show such a periodic motion pattern.

Running is a state of motion of walking, and when the speed reaches a certain point, walking becomes running. There are both similarities and differences between them. The similarity is that their gait cycles are the same, and the difference is reflected in the fact that both feet cannot be supported at the same time when running and there is a period of vacating. Running is divided into six cycles: left foot support period, right foot vacating period, swing period, right foot support period, left foot vacating period, and swing period. The change of the motion state of running is like that of walking mentioned above, and the posture angle calculated from the posture sensor verifies this theory. As shown in Figure 3, the posture angle graphs of the two motions have similar trends, but the magnitude of the

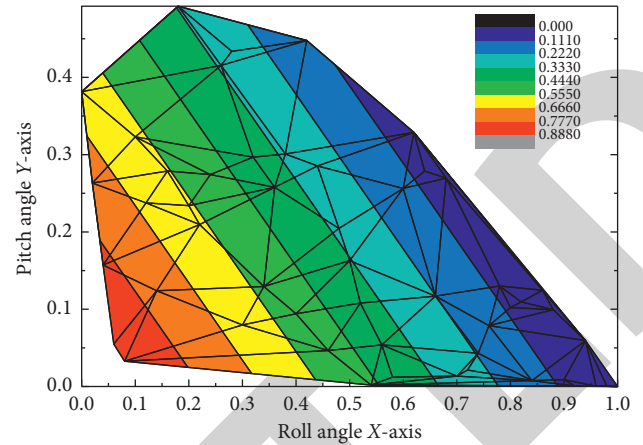


FIGURE 3: Running and walking posture angles.

changes is different, which is not enough to characterize both. Therefore, the identification of these two states is not considered in terms of attitude angle for the time being.

According to a large amount of previous experimental data, human gait motion is mainly low-frequency signals, and the signals generated by running and walking are in the low-frequency band. The amplitude of running is higher than that of walking up and down the stairs, and the amplitude of walking is the lowest. Y-axis acceleration signal amplitude is lower after FFT transformation and cannot be distinguished.

The Gaussian mixture model is a mixture model based on Gaussian distribution, which is equivalent to a weighted average of several Gaussian probability density functions, where each Gaussian density function is a model and the parameters are all independent of each other. When each model has enough data, it can approximate an arbitrary random distribution with high accuracy and can describe the distribution properties of the data. When the random variables satisfy the following probability distributions, they can be called Gaussian mixture models.

$$P(X, \theta) = \lim_{k \rightarrow \infty} \sum_{j=1}^k \alpha_j \varphi(X, \theta_j)^2, \quad (7)$$

where  $\alpha_j$  is the probability that the random variable  $X$  obeys the probability density function and satisfies  $\alpha_j > 0$  and  $\varphi(X, \theta_j)$  is a Gaussian distribution density function consistent with the parameters  $\theta_j = (u_j, \sigma_j^2)$ ; the probability density function is expressed as

$$f(x) = \frac{1}{\sqrt{2\pi\sigma^2}} e^{-(x-u)^2/2\pi\sigma^2}. \quad (8)$$

There is also a dirty data phenomenon that is very easy to appear in the combined data, that is, due to the natural flaws in the acquisition principle of one or more characteristic variables in the data, all or a significant proportion of the data in this dimension have the phenomenon of erroneous data. Under the premise that it cannot be processed or the processing cost is huge, the variable type can be considered to be discarded. For example, in this experiment, the

temperature variable output from the IMU device was discarded because the conditions for controlling the temperature variable were not available, and the effect of this part of the data on the action expression was not investigated. Since IMU devices are often used for navigation purposes such as heading reference, they generally output attitude solving results [26, 27]. However, since inertial devices measure the attitude of a moving object indirectly, the gyroscope sensor measures only the relative angular rate, and since the carrier coordinate system itself is constantly changing with rotation, the relative angle obtained by integrating the gyroscope output cannot be used directly as an expression of the attitude in the inertial system. It can only be used as the update data of the attitude matrix to indirectly solve the attitude expression of the carrier in the inertial system. The sampling frequency of digital devices cannot be increased infinitely, so performing discrete integration operations will make the attitude information contain principal errors, and the accumulation of errors will become more serious as the integration time increases [28, 29]. Since the motion durations studied in this project are relatively short and the accumulation of errors is manageable, it can be approximated that the accuracy of the inertial device output is sufficient to accurately describe a small range of human joint motion, as shown in Figure 4.

The processing of human posture data is also implemented in the software side of the upper computer; after the initialization of the upper computer is completed, the receiver side of the communication module begins to receive human action data, first, the data preprocessing process; after the completion of preprocessing, it should be the first time to determine whether this packet is correct; if the packet is the wrong, data is discarded. The correct data packet will continue to the next step of processing; that is, the sensor data is calculated and fused with the angle value; the angle value is an important reference indicator for the update of the human body model. Before sending the angle value to the human body model, we need to judge the source of the packet and distribute it to the corresponding part of the human body model according to the source of the data and replot and trace the line according to the angle value to complete the real-time update of the human body model.

## 4. Results and Discussion

*4.1. Wearable Sensor Network Performance Results.* First, for the process of wearing the motion capture module, according to the system requirements of each module strapped to the corresponding position of the limb, the sensor is located at the wrist and ankle; confirm the orientation of the sensor to ensure the accuracy of data acquisition; four motion-capture modules wearing is completed to turn on the switch, ready to collect posture data. Then open the upper computer software, and click the button “Connect” button to check whether the human stick model is normal and changes in real time with the limb swing. After the motion capture is completed, click the “Disconnect” button to disconnect the sensor unit from the host software. Finally, the motion capture process is completed and the motion capture effect is viewed. In the

experiment, the time delay is defined as the time required for the host software to complete the polling of the four nodes after the motion capture unit data is updated. The test scheme is as follows: set the operation mode of the motion capture unit so that it will send 11 bytes of data immediately after receiving the convergence node command (the length of the motion capture unit data packet is 11 bytes). At the same time, a timer is set in the host computer software to start the timer when polling is started, and the timer is stopped and the time is recorded when 100 polls are completed. The average time delay of the system is 258.79 ms, which can be calculated from the test results in Figure 5.

After the hardware circuit and each subroutine design is completed, the overall test of the motion capture system is carried out, which mainly contains five parts: toolbar, main program interface, solution explorer, output box, and property box, after the software engineering is established and the program is written. The left side of the upper computer interface is the human stick model, and the right side is the function buttons and data display window. After testing, the human stick model can reproduce the action of human limbs waving, and the real time is good, and no obvious time delay can be observed by naked eyes. The buttons on the right side of the window are simple, intuitive, and functionally sensitive, and the data display window shows the data of each sensor in real time. Before the sensor is worn, the inertial sensor is first turned on and placed at rest for a period to complete the calibration of the gyroscope, and then the magnetometer is calibrated by drawing  $\infty$  the shape in the air, and the attitude of the sensor is collected at 100 Hz. The inertial sensor is fixed to the corresponding limb using an elastic bandage to ensure that no relative movement occurs during human movement. Once everything is ready, the experimenter follows the prompts to perform three calibration poses in sequence, holding each pose for at least three seconds, as shown in Figure 6.

In Figure 6, the topmost is the pose quadratic curve of the right forearm, the middle is the pose fluctuation curve of the right forearm before filtering, and the bottom is the pose fluctuation wireless of the right forearm after filtering. According to the experimental results, the width of the sliding window is set to  $W=60$ , and the sliding window average can significantly reduce the effect of arm jitter on the calibration pose segmentation. When the amplitude of the human arm jitter is relatively large, the posture fluctuation threshold can be increased to avoid the phenomenon of misclassification.

However, from the actual implementation results, the effect of dimensionality reduction using the PCA method is not very outstanding, and the recognition accuracy has been reduced to about 93% at only 18% feature dimensionality reduction, which shows that the previously obtained streamlined feature combination is already a more compact form of expression for the intrinsic properties of the data. Such experimental results, although not consistent with the prediction, argue against the rigor and reliability of the feature screening scheme introduced in the previous paper.

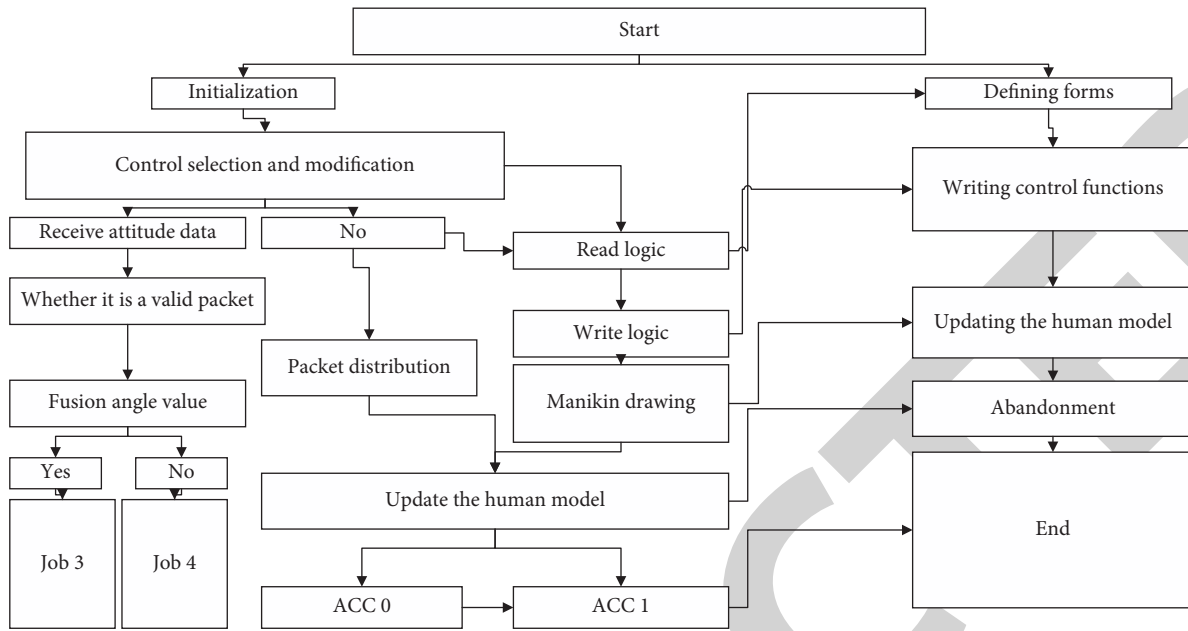


FIGURE 4: Overall flowchart of motion capture.

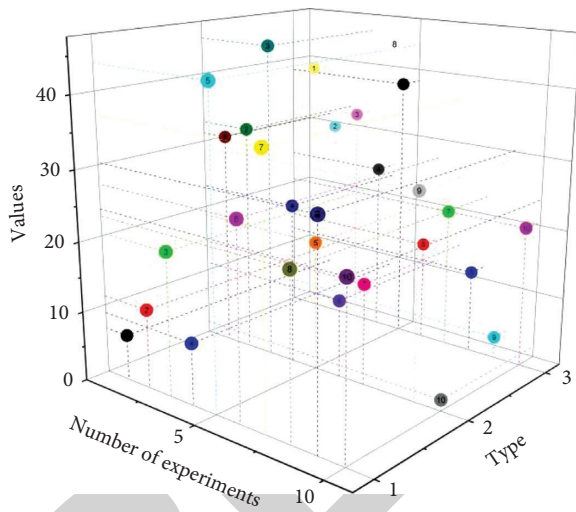


FIGURE 5: System delay test results.

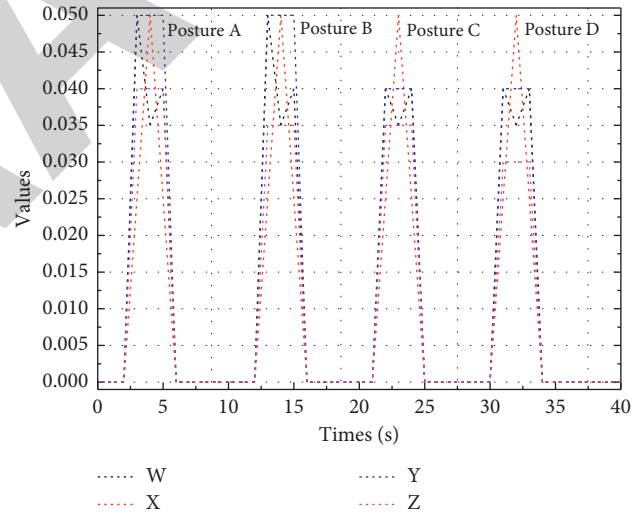


FIGURE 6: Segmentation of the calibration pose.

4.2. Analysis of Dance Motion Capture Algorithm Results. Repeating this step over and over, the training set data are all input to the environment for model learning training, if the parameters that match the Gaussian distribution function of each data are classified into the relevant gesture actions when a certain data is an input. The approximate Gaussian distribution parameters for each gesture are counted according to the comparison earlier in the article. Inputting a set of 4 data gestures into the Python environment, because the parameters of each gesture data are different, combined with the previous features of each gesture model, the 4 gestures will be roughly distinguished, and although there is some data overlap, the distribution of the 4 gestures is still different, as shown in Figure 7.

To further verify the accuracy of human motion capture, this experiment uses the single-axis rotational motion of the joint to evaluate it. When the joint does uniaxial rotational motion, the joint angles of the other two axes should be close to zero except for a large change in the joint angle of the motion axis. Due to the influence of muscle involvement during human movement, the joint angles of nonmotor axes also fluctuate in small angles, and the smaller value indicates the higher accuracy of human motion capture. Take the elbow joint extension/flexion motion as an example, the upper arm is kept stationary, and the forearm does extension/flexion round-trip motion around the elbow joint, and try to ensure that the elbow joint does not have internal/external abduction motion and internal/external rotation

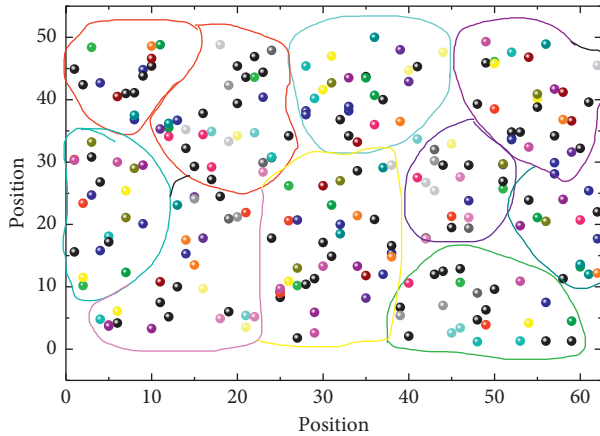


FIGURE 7: Four types of data classification.

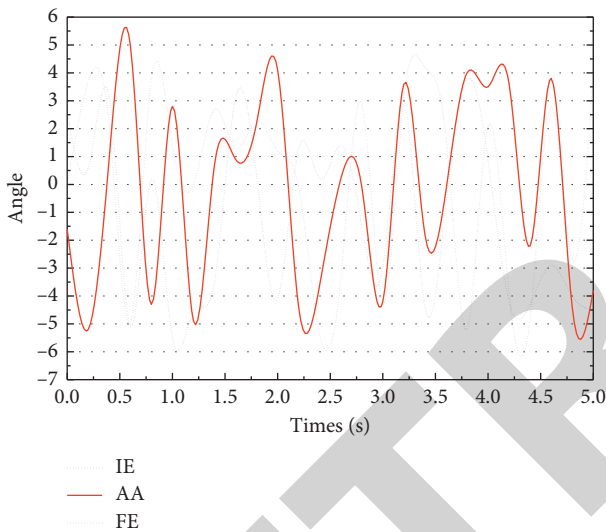


FIGURE 8: Articular motion of the knee joint of the right leg.

motion during the motion. Figure 8 shows the postures of the upper arm and forearm during the extension/flexion round-trip motion of the elbow joint and the three joint angles of the elbow joint during the extension/flexion round-trip motion.

For the same gesture signal, the random template selection method corresponds to the lowest recognition rate and the ADBA time-series averaged template selection method corresponds to the highest recognition rate. The gesture templates selected by the random template selection method cannot fully reflect all the features of the gestures, and therefore their recognition rates are relatively low. The recognition rate based on the time-series averaged template selection method is much higher than that of the random template selection method and the most similar template selection method. Since the ADBA algorithm can average the gesture sequences in both time and space, its recognition rate is much higher than the other two time-series averaging template selection methods.

To evaluate the human action recognition algorithm proposed in this chapter, 3600 gesture samples were

collected, all of which were right-handed gestures. Five experimenters participated in this experiment, three of them were male and the remaining two were female. The average age of the experimenters was 24 years old and they had no upper limb motor disorders. Considering the variability of the experimenter's gestures in different periods, the experiment was divided into six days for data collection, and each gesture was repeated 10 times in each day of the acquisition experiment. During the gesture signal acquisition, information on the posture, linear acceleration, angular velocity, and accelerometer measurements during the arm movement is collected simultaneously. The calibration algorithm also provides feedback on the calibration quality, which is considered unsuccessful when it exceeds a present threshold and reminds the user to recalibrate. For the human parameter estimation problem, two human parameter estimation methods are proposed in this chapter. The first method uses human joint constraints to estimate joint parameters and limb lengths, and the second method estimates limb lengths by forming a closed joint chain with two different limb ends. The experimental results show that the estimation of human parameters based on the closed joint chain is more accurate. In this chapter, a wearable human motion capture system software and hardware platform are built using nine-axis MEMS inertial sensors and UWB sensors. Experimental results show that the wearable human motion capture system designed in this paper can capture and reconstruct human motion accurately and in real time.

## 5. Conclusions

The inertial sensor is first calibrated and the calibration parameters are used to compensate for the measurement output of the sensor and reduce the impact of sensor measurement errors on attitude measurement. The attitude estimation algorithm proposed in this paper can be divided into two layers: inner and outer. The inner layer calculates the a priori estimate of the attitude quaternion by integrating the angular velocity of the gyroscope output, and the update frequency of the inner layer can be very high due to the high output frequency of the gyroscope combined with the small computation. The outer layer is an extended Kalman filter based on the error quaternion, which first uses the error quaternion process model and gyroscope measurements to calculate the a priori estimate of the error quaternion and then calculates the posteriori estimate of the error quaternion based on accelerometer and magnetometer measurements. To address the many problems faced by optical motion capture systems, this paper uses wearable sensors to build a low-cost, high-precision, easy-to-wear, and simple-to-operate human motion capture system and uses the motion capture data to realize the recognition of human motion. The experimental results of gesture recognition show that the recognition rate based on gesture motion sequences is much higher than that of gesture acceleration sequences and gesture angular rate sequences, and the template creation method proposed in this chapter is significantly better than other template selection methods, and its user-related recognition rate

and user-irrelevant recognition rate are 99.2% and 96.9%, respectively. In this paper, the research focuses on human motion capture and recognition based on wearable sensors and proposes a multisensor fusion-based pose and position estimation algorithm, an initialization calibration algorithm, and a template matching-based human motion recognition algorithm and builds a wearable human motion capture system hardware and software platform to verify the effectiveness of the above algorithms. Our existing research is not yet applicable to practice, and later, we further optimize the existing research results so that the model can be used in practice.

## Data Availability

The data used to support the findings of this study are available from the corresponding author upon request.

## Conflicts of Interest

The author declares no conflicts of interest.

## References

- [1] J. S. Olson and S. Redkar, "A survey of wearable sensor networks in health and entertainment," *MOJ Applied Bionics and Biomechanics*, vol. 2, no. 5, pp. 280–287, 2018.
- [2] F. Zhang, T.-Y. Wu, J.-S. Pan, G. Ding, and Z. Li, "Human motion recognition based on SVM in VR art media interaction environment," *Human-centric Computing and Information Sciences*, vol. 9, no. 1, pp. 1–15, 2019.
- [3] A. Z. Md Faridee, S. R. Ramamurthy, N. Roy, and N. Roy, "HappyFeet," *GetMobile: Mobile Computing and Communications*, vol. 22, no. 3, pp. 10–16, 2019.
- [4] S. Shimada, V. Golyanik, W. Xu, and C. Theobalt, "PhysCap," *ACM Transactions on Graphics*, vol. 39, no. 6, pp. 1–16, 2020.
- [5] D. V. Fedasyuk and T. A. Marusenkova, "An algorithm for detecting the minimal sample frequency for tracking a preset motion scenario," *International Journal of Intelligent Systems and Applications*, vol. 12, no. 4, pp. 1–12, 2020.
- [6] J. Lu, X. Zheng, M. Sheng, J. Jin, and S. Yu, "Efficient human activity recognition using a single wearable sensor," *IEEE Internet of Things Journal*, vol. 7, no. 11, pp. 11137–11146, 2020.
- [7] R. Kaushik and A. LaViers, "Imitation of human motion by low degree-of-freedom simulated robots and human preference for mappings driven by spinal, arm, and leg activity," *International Journal of Social Robotics*, vol. 11, no. 5, pp. 765–782, 2019.
- [8] D. St-Onge, U. Côté-Allard, K. Glette, B. Gosselin, and G. Beltrame, "Engaging with robotic swarms: commands from expressive motion," *ACM Transactions on Human-Robot Interaction*, vol. 8, no. 2, pp. 1–26, 2019.
- [9] D. Kim, J. Kwon, S. Han, Y.-L. Park, and S. Jo, "Deep full-body motion network for a soft wearable motion sensing suit," *IEEE/ASME Transactions on Mechatronics*, vol. 24, no. 1, pp. 56–66, 2018.
- [10] A. Switonski, H. Josinski, and K. Wojciechowski, "Dynamic time warping in classification and selection of motion capture data," *Multidimensional Systems and Signal Processing*, vol. 30, no. 3, pp. 1437–1468, 2019.
- [11] H. Malik and A. Mazhar, "EyeCom: an IoT based affordable wearable solution for paralyzed people to interact with machines," *Journal of Ambient Intelligence and Humanized Computing*, vol. 11, no. 6, pp. 2325–2336, 2020.
- [12] V. Santhanam and D. B. Shanmugam, "Integrating wireless sensor networks with cloud computing and emerging IT platforms using middleware services," *International Research Journal of Engineering and Technology*, vol. 5, no. 8, pp. 804–823, 2018.
- [13] S. Liaqat, K. Dashtipour, K. Arshad, K. Assaleh, and N. Ramzan, "A hybrid posture detection framework: integrating machine learning and deep neural networks," *IEEE Sensors Journal*, vol. 21, no. 7, pp. 9515–9522, 2021.
- [14] A. Mosenia, S. Sur-Kolay, A. Raghunathan, and N. K. Jha, "Wearable medical sensor-based system design: a survey," *IEEE Transactions on Multi-Scale Computing Systems*, vol. 3, no. 2, pp. 124–138, 2017.
- [15] S. Gashi, E. Di Lascio, and S. Santini, "Using unobtrusive wearable sensors to measure the physiological synchrony between presenters and audience members," *Proceedings of the ACM on Interactive, Mobile, Wearable and Ubiquitous Technologies*, vol. 3, no. 1, pp. 1–19, 2019.
- [16] K. E. Raheb, M. Stergiou, A. Katifori, and Y. Ioannidis, "Dance interactive learning systems: a study on interaction workflow and teaching approaches," *ACM Computing Surveys*, vol. 52, no. 3, pp. 1–37, 2019.
- [17] S. Senecal, N. A. Nijdam, A. Aristidou, and N. Magnenat-Thalmann, "Salsa dance learning evaluation and motion analysis in gamified virtual reality environment," *Multimedia Tools and Applications*, vol. 79, no. 33, pp. 24621–24643, 2020.
- [18] Y. Lu and S. Velipasalar, "Autonomous human activity classification from wearable multi-modal sensors," *IEEE Sensors Journal*, vol. 19, no. 23, pp. 11403–11412, 2019.
- [19] W. Zhuang, S. Xu, Y. Han, J. Su, C. Gao, and D. Yang, "The design and implementation of a wearable human activity recognition system based on IMU," *International Journal of Embedded Systems*, vol. 13, no. 2, pp. 158–168, 2020.
- [20] M. Chen, Y. Jiang, Y. Cao, and A. Y. Zomaya, "CreativeBioMan: a brain-and body-wearable, computing-based, creative gaming system," *IEEE Systems, Man, and Cybernetics Magazine*, vol. 6, no. 1, pp. 14–22, 2020.
- [21] A. Nabil, H. Hegazy, A. Mohamed et al., "Usability Study of a comprehensive table tennis AR-based training system with the focus on players' strokes," *Journal of Ubiquitous Systems and Pervasive Networks*, vol. 13, no. 1, pp. 01–09, 2020.
- [22] F. Onorati, G. Regalia, C. Caborni et al., "Multicenter clinical assessment of improved wearable multimodal convulsive seizure detectors," *Epilepsia*, vol. 58, no. 11, pp. 1870–1879, 2017.
- [23] C. Gong, Y. Hu, J. Gao et al., "An improved delay-suppressed sliding-mode observer for sensorless vector-controlled PMSM," *IEEE Transactions on Industrial Electronics*, vol. 67, no. 7, pp. 5913–5923, 2019.
- [24] Z. Wang, J. Li, J. Wang et al., "Inertial sensor-based analysis of Equestrian sports between beginner and professional riders under different horse gaits," *IEEE Transactions on Instrumentation and Measurement*, vol. 67, no. 11, pp. 2692–2704, 2018.
- [25] W. Wei, E. S. L. Ho, K. D. McCay et al., "Assessing facial symmetry and attractiveness using augmented reality," *Pattern Analysis and Applications*, pp. 1–17, 2021.
- [26] S. Qiu, Z. Wang, H. Zhao, and H. Hu, "Using distributed wearable sensors to measure and evaluate human lower limb motions," *IEEE Transactions on Instrumentation and Measurement*, vol. 65, no. 4, pp. 939–950, 2016.

- [27] Y. Yang, Y. Song, X. Bo et al., "A laser-engraved wearable sensor for sensitive detection of uric acid and tyrosine in sweat," *Nature Biotechnology*, vol. 38, no. 2, pp. 217–224, 2020.
- [28] A. Alsiddiky, W. Awwad, H. Fouad et al., "Priority-based data transmission using selective decision modes in wearable sensor based healthcare applications," *Computer Communications*, vol. 160, pp. 43–51, 2020.
- [29] J. Yang, S. Xiao, B. Jiang et al., "Cache-enabled unmanned aerial vehicles for cooperative cognitive radio networks," *IEEE Wireless Communications*, vol. 27, no. 2, pp. 155–161, 2020.

RETRACTED